Check for updates

Detection of hypochlorous acid fluctuation *via* a selective fluorescent probe in acute lung injury cells and mouse models†

Na He,[a] Yude Wang,[b] Yan Huang,[bc] Lingxin Chen, ✓ *[c] Xiaoyan Wang,[bc] Changjun Lv*[b] and Shouwei Yue*[a]

Acute lung injury (ALI) is a diffuse inflammatory pulmonary damage caused by excessive ROS that break the coordination of normal physiological structures and functions. Hypochlorous acid (HOCl), one kind of ROS, is a hopeful biological marker for inflammation-related diseases. Therefore, the excessive generation of HOCl might be a significant reason for oxidative injury in ALI. Herein, we developed a fluorescent probe, namely BCy-HOCl, for quantitatively monitoring and visualizing HOCl in living cells and *in vivo*. The probe BCy-HOCl displayed a significant fluorescence signal enhancement towards HOCl with excellent selectivity and sensitivity. The variation of HOCl in the ALI cell model and ALI mouse model was evaluated with BCy-HOCl to clarify the relationship between ALI and HOCl. Our results verified that the HOCl levels conspicuously increased with the severity of the ALI. Thus, HOCl is likely to play a crucial part in the process of ALI, which will probably provide a new strategy for its treatment.

1. Introduction

Acute lung injury (ALI), an inflammation-related disease in pulmonary tissue, is caused by multiple etiological factors *in vitro* and *in vivo*,[1] of which the most serious form is acute respiratory distress syndrome (ARDS). The inflammation-induced injury to the alveolar capillary endothelial and epithelial cells causes lung hemorrhage and edema that are the major pathological characteristics of ALI.[2] Despite extensive research, the pathogenesis and treatment of ALI reports a mortality rate of 22–58%, which justifies the need of studying this disease in depth.[3] Previous studies have indicated that excessive inflammation was the most detrimental reason for ALI, and oxidative stress played a crucial role in the progression of ALI including its transition to ARDS.[4] Therefore, it is currently widely accepted that reducing inflammation is the most useful therapy for ALI.[5] As a result, ROS excessively generated in the lungs can cause the occurrence and

aggravation of ALI. ROS, as essential signaling molecules, are well known as important players in numerous physiological processes and stress responses. Under the catalysis of myeloperoxidase (MPO), hypochlorous acid (HOCl), a type of ROS, is produced in immune cells by an effective reaction between chloride ions and hydrogen peroxide.[6] HOCl participates in various physiological processes of the immune system, which includes regulating cellular apoptosis, inhibiting inflammatory responses and antagonizing pathogens.[7,8] More importantly, the correlation between the amount of HOCl and the inflammation-associated disorder has been illustrated,[9] but the connection between ALI and HOCl has not been fully revealed so far. We believe that the fluctuation in the cellular HOCl level is one of the major causes for ALI damage. Therefore, it is still necessary to establish a desirable method for detecting HOCl levels as well as exploring the correlation between ALI and HOCl.

Further studies on the oxidation function of HOCl have been limited vastly due to the handicap of detecting accurately such a small molecule in complex biological organisms, prompting researchers to design methods with high sensitivity and selectivity for monitoring HOCl, to afford accurate and effective HOCl signal changes, both in living cells and *in vivo*.[10] Fluorescence imaging has become a crucial approach for sensing biological molecules in biological systems owing to its capability of real-time analysis and excellent selectivity and sensitivity. Previously, multiple fluorescent probes to detect

[a] *Rehabilitation Center, Qilu Hospital, Cheelo College of Medicine, Shandong University, Jinan 250100, China. E-mail: shouweiy@sdu.edu.cn*

[b] *Department of Respiratory Medicine, Binzhou Medical University Hospital, Binzhou 256603, China. E-mail: lucky_lcj@sina.com*

[c] *CAS Key Laboratory of Coastal Environmental Processes and Ecological Remediation, The Research Center for Coastal Environmental Engineering and Technology, Yantai Institute of Coastal Zone Research, Chinese Academy of Sciences, Yantai 264003, China. E-mail: lxchen@yic.ac.cn*

† Electronic supplementary information (ESI) available. See DOI: 10.1039/d0tb01969k

This journal is © The Royal Society of Chemistry 2020

J. Mater. Chem. B, 2020, **8**, 9899–9905 | **9899**

HOCl have been synthesized, most of which were designed in the light of the combination of a HOCl-recognizing moiety and an organic fluorophore, including thiol, dibenzoyl hydrazine, hydroxamic acid, N-heterocyclic carbene borane, ferrocene and oxime derivatives.[11–37] In recent years, we have committed to developing new fluorescent probes for bioimaging HOCl in complex biological environments, particularly those used to detect the HOCl produced under hypoxic stress.[38] As a part of our ongoing study, we recently centered our efforts on a fluorescent probe that is simple to synthesize in high yield, provides high sensitivity and a good selectivity for evaluating the detailed function of HOCl in the ALI process.

Herein, we developed a probe BCy-HOCl for detecting HOCl in living cells and *in vivo*. The probe contains two moieties: a dimethylthiocarbamate group as the response unit and a benzoindocyanine fluorophore as the fluorescence modulator. The treatment of the benzoindocyanine fluorophore with dimethylthiocarbamoyl chloride afforded the BCy-HOCl probe in good yield. With high selectivity and sensitivity, BCy-HOCl displays specific fluorescence enhancement towards HOCl. By monitoring HOCl in living cells, the potential of BCy-HOCl as a HOCl biosensor was demonstrated. Furthermore, BCy-HOCl was successfully utilized for the specific bioimaging of HOCl *in vivo*. The results confirmed that the HOCl levels were obviously increased in two types of ALI cell models and two corresponding ALI animal models. The potential connection between the HOCl level and the degrees of ALI was validated. HOCl might play a significant part in the process of ALI. For all we know, BCy-HOCl was the first fluorescent tool for the investigation of the correlation between the HOCl level and ALI in living cells and living mice. We anticipated that our BCy-HOCl probe will serve as a powerful fluorescent tool for studying the biological role of HOCl in biological systems.

2. Experimental

2.1 Synthesis of the BCy-HOCl probe

Cesium carbonate (0.326 g, 1 mmol) and compound BCy (0.469 g, 1 mmol) were dissolved in dichloromethane. Under nitrogen at room temperature, we stirred the mixture. After 30 min, we added dimethylthiocarbamoyl chloride to the mixture (210 μL). The dimethylthiocarbamoyl chloride (200 μL) was added twice a day during the next 3 days of stirring. Using CH_2Cl_2/CH_3OH (9:1, v/v) as an eluent, the crude product was purified *via* silica gel chromatography. Finally, we get a yellow product BCy-HOCl (0.333 g, 60% yield). ^1H NMR (500 MHz, CD_3OD-D_4) δ (ppm): 8.55 (d, 1H), 8.43–8.41 (d, 1H), 8.26–8.19 (m, 4H), 8.04–8.02 (m, 1H), 7.94–7.91 (m, 1H), 7.84–7.81 (m, 1H), 7.73–7.70 (m, 1H), 7.38–7.29 (m, 2H), 3.39–3.32 (m, 2H), 3.16–3.04 (m, 6H), 2.10 (s, 6H), 1.68–1.65 (t, 3H). ^{13}C NMR (125 MHz, CD_3OD-D_4) δ (ppm): 191.92, 191.85, 186.48, 182.56, 158.05, 155.58, 154.43, 152.59, 152.56, 139.19, 137.85, 134.00, 131.57, 131.26, 129.97, 128.34, 127.37, 127.23, 123.89, 122.89, 122.54, 112.34, 54.28, 42.76, 42.24, 37.85, 35.67, 35.55, 25.03, 13.10. MS (ESI): m/z calcd for $C_{27}H_{29}N_2OS^+$ $[M]^+$ 429.20, found 429.42.

2.2 Cytotoxicity of BCy-HOCl

Using the MTT assay, we checked the cytotoxicity of BCy-HOCl. A549 cells (human alveolar epithelial cells) and RLE-6TN cells (rat type two alveolar epithelial cells) were carefully seeded to a 96-well cell culture plate at an end density of 8×10^3 cells each well. We added various concentrations of BCy-HOCl (0.1, 1, 10 and 100 mM) to each wells separately. The A549 cells and RLE-6TN cells were treated at 37 °C for 24 h. Subsequently, we added MTT to each well (final concentration 5 mg mL^{-1}) for 4 h. Next, formazan crystals formed, which were adequately dissolved in DMSO (150 mL). *Via* a microplate reader, the MTT formazan was directly quantified by absorbance (OD) at 570 nm. According to Huber and Koella, the calculation of IC$_{50}$ values were finished. The experimental data are the average standard deviation of six independent measurements.

2.3 ALI cell models

For the establishment of ALI cell models stimulated by LPS, A549 cells were stimulated with lipopolysaccharide (LPS 500 μM) for 24 h. Before imaging, the control cells and ALI cell models were treated with BCy-HOCl at 37 °C for 30 min. For the establishment of ALI cell models induced by hyperoxia, RLE-6TN cells were treated with H_2O_2 (500 mM) for 24 h. Then, before imaging, the control cells and ALI cell models were treated with BCy-HOCl at 37 °C for 30 min.
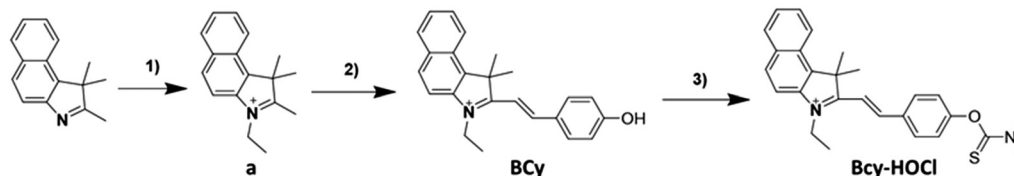
2.4 ALI mouse models

For the establishment of LPS-induced ALI mouse models, C57BL/6 mice were given LPS (1 mg kg^{-1}) for 24 h through intranasal administration. For the establishment of hyperoxia-induced ALI mouse models, C57BL/6 mice were adequately exposed to high levels of oxygen for 48 h, which were carried out in an airtight plastic chamber with oxygen flow rates of around 5.0 L min^{-1} to maintain the oxygen concentration ($\geq$95%); granular soda lime was applied in the chamber to reduce the CO_2 level ($\leq$5%). BCy-HOCl was administered intratracheally 1 h before taking the imaging *in vivo*. Afterwards, all C57BL/6 mice in this study were killed. For further experiments, the collected tissue sections were rapidly frozen in liquid nitrogen. All experimental procedures were conducted in conformity with institutional guidelines for the care and use of laboratory animals, and the protocols were approved by the Institutional Animal Care and Use Committee in Binzhou Medical University, Yantai, China. Approval number: no. BZ2014-102R.

3. Results and discussion

3.1 Design strategies for the BCy-HOCl probe

The design approach of the BCy-HOCl probe is shown in Scheme 1. In the experimental part, the specific steps for the synthesis of all compounds are displayed. The mechanism for the BCy-HOCl synthesis is exhibited in Scheme 2. All the compounds were characterized *via* ^1H NMR, ^{13}C NMR and MS. A benzoindocyanine dye (BCy), as the fluorophore unit, was applied for emitting the signal at the emission wavelength

9900 | *J. Mater. Chem. B*, 2020, **8**, 9899–9905

This journal is © The Royal Society of Chemistry 2020

Scheme 1 Synthetic approach of BCy-HOCl. (1) Benzoiodoethane, acetonitrile, refluxed, 12 h, 90%; (2) 4-hydroxybenzaldehyde, ethanol, reflux, 48 h, 84%; (3) dimethylthiocarbamoyl chloride, cesium carbonate, CH_2Cl_2, room temperature, 3 d, 60%.
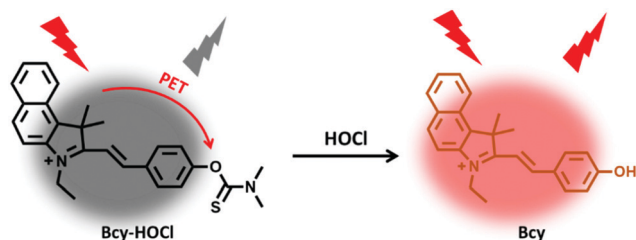
Scheme 2 Proposed detection mechanism of probes against HOCl.

of 630 nm. To get the BCy-HOCl probe for detecting HOCl, we incorporated the specific recognition moiety of the dimethylthiocarbamoyl group into the fluorophore unit. In particular, the dimethylthiocarbamoyl group as the response unit of HOCl shows specific response and high sensitivity.[39] For the construction of the target probe, the emission of BCy was quenched by the dimethylthiocarbamoyl group due to the photo-induced electron-transfer (PET) mechanism, so the BCy-HOCl probe was almost non-fluorescent. When HOCl recognizes dimethylthiocarbamoyl in BCy-HOCl, the sulfite bond is cleaved leading to BCy, which in turn results in a fluorescence enhancement. With BCy-HOCl, we would monitor the changes of HOCl in biological environment in real-time. Furthermore, the physiological function of HOCl in the development process of ALI would be excavated.

3.2 Spectroscopic properties

Under a simulated physiological environment (10 mM HEPES buffer, pH = 7.4), the spectral response of BCy-HOCl to HOCl was checked. The maximum absorption wavelength for BCy-HOCl is located at 450 nm. BCy-HOCl displays an obvious red shift at 500 nm upon the addition of HOCl (Fig. 1a). Next, for testing the fluorescence response of BCy-HOCl towards HOCl,
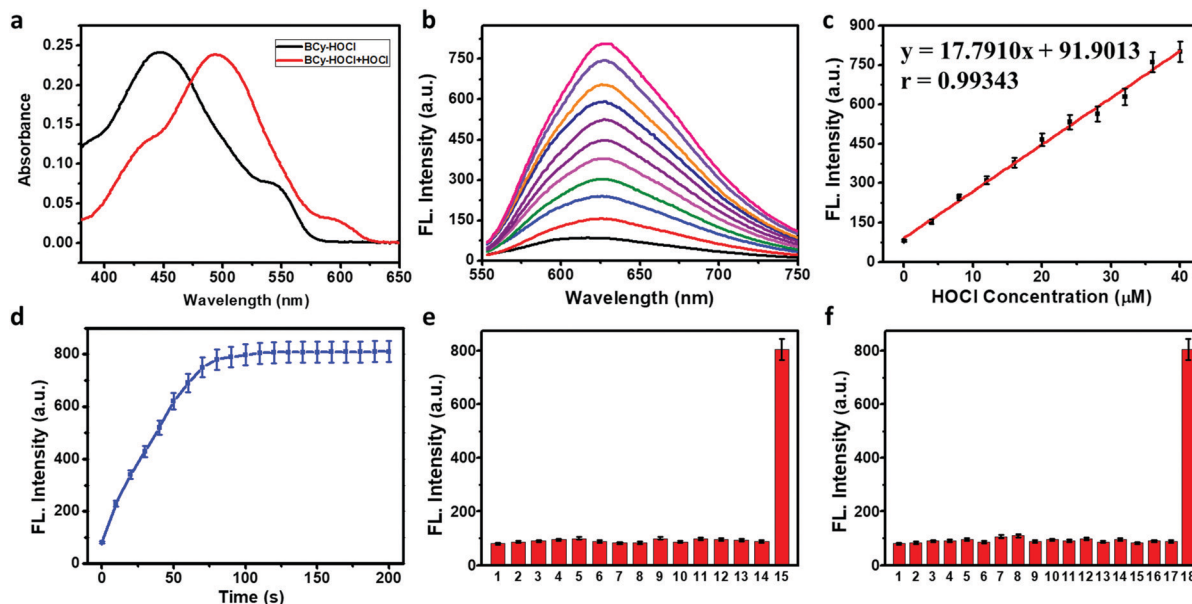

Fig. 1 Spectral properties of BCy-HOCl. (a) Absorption spectral changes of BCy-HOCl (5 μM) in the presence of NaClO (40 μM). (b) Fluorescence emission spectral variation of BCy-HOCl (5 μM); spectra displays distinct added concentrations of NaClO (0−40 μM). (c) The plot of the linear relationship between the fluorescence intensities and NaClO concentrations (0−40 μM). (d) Plot of the fluorescence intensity of BCy-HOC (5 μM) vs. the reaction time with NaClO (30 μM). (e) Fluorescence responses of BCy-HOCl (5 μM), to various metal ions and anions: (1) blank; (2) Na^+ (1.0 mM); (3) Ca^{2+} (1.0 mM); (4) Mg^{2+} (1.0 mM); (5) Zn^{2+} (1.0 mM); (6) Cu^{2+} (1.0 mM); (7) Cl^- (1.0 mM); (8) Br^- (1.0 mM); (9) HSO_3^- (100 μM); (10) SO_4^{2-} (100 μM); (11) SO_3^{2-} (100 μM); (12) $S_2O_3^{2-}$ (100 μM); (13) CO_3^{2-} (100 μM); (14) $H_2PO_4^{2-}$ (100 μM); (15) NaClO (30 μM). (f) Fluorescence response of BCy-HOC (5 μM) towards various biospecies. (1) Blank, (2) S-nitrosoglutathione (GSNO) (100 μM), (3) $ONOO^-$ (100 μM), (4) NO (NOC-5) (100 μM), (5) NO_2^- (100 μM), (6) tocopherols (100 μM), (7) H_2O_2 (100 μM), (8) $O_2^{•-}$ (100 μM), (9) methyl linoleate hydroperoxide (100 μM), (10) Na_2S_4 (a donor of H_2S_n) (100 μM), (11) L-cysteine (L-cys) (100 μM), (12) glutathione (GSH) (100 μM), (13) NaHS (100 μM), (14) ascorbic acid (100 μM), (15) L-arginine (L-arg) (100 μM), (16) tyrosine (100 μM), (17) hydroxylamine (HA) (100 μM), (18) NaClO (30 μM). Data were gathered at λ_{ex} = 500 nm, λ_{em} = 630 nm.

This journal is © The Royal Society of Chemistry 2020

J. Mater. Chem. B, 2020, **8**, 9899−9905 | **9901**

we examined the fluorescence spectra of BCy-HOCl. In Fig. 1b, an increase in the fluorescence emission at 630 nm occurred after the addition of HOCl (from 0 to 40 μM) at the excitation wavelength of 500 nm. Thus, we chose emission at 630 nm for quantifying the fluorescence response of BCy-HOCl towards HOCl. Fig. 1c displays the calibration curve, which shows a great linearity towards HOCl (from 0 to 40 μM), being the regression equation $F_{630nm} = 17.7910 \times [HOCl]$ (μM) + 91.9013 ($r = 0.9934$). The minimum concentration of HOCl in the linear correlation is 0.2 μM. The limit of detection (3 s per slope) towards HOCl was 17 nM under the simulated conditions. The data revealed that BCy-HOCl was able to monitor HOCl with excellent sensitivity. BCy-HOCl has a great application potential in biological samples.

3.3 Kinetic investigation of BCy-HOCl towards HOCl

Considering the unstable properties and rapid metabolic characteristics of HOCl in biologically relevant systems, a rapid response provides the feasibility of its real-time detection in living cells and *in vivo*. The activity of HOCl towards BCy-HOCl was subsequently evaluated. In Fig. 1d, we show the fluorescence kinetic curves of BCy-HOCl (5 μM) with HOCl (30 μM) for 200 s, where BCy-HOCl displayed a rapid response rate and obvious fluorescence increase. The fluorescence intensity in this experiment reached a plateau in about 80 s. These results indicate that BCy-HOCl had the capability of rapidly and successively responding to HOCl.

3.4 Selectivity of BCy-HOCl towards HOCl

Next, the fluorescence response of BCy-HOCl towards other biologically related species was investigated. As indicated in Fig. 1e, BCy-HOCl was incubated with a variety of metal ions and anions: (1) blank; (2) Na^+ (1.0 mM); (3) Ca^{2+} (1.0 mM); (4) Mg^{2+} (1.0 mM); (5) Zn^{2+} (1.0 mM); (6) Cu^{2+} (1.0 mM); (7) Cl^-

(1.0 mM); (8) Br^- (1.0 mM); (9) HSO_3^- (100 μM); (10) SO_4^{2-} (100 μM); (11) SO_3^{2-} (100 μM); (12) $S_2O_3^{2-}$ (100 μM); (13) CO_3^{2-} (100 μM); (14) $H_2PO_4^{2-}$ (100 μM); (15) NaClO (30 mM). As indicated in Fig. 1f, the BCy-HOCl probe was incubated with a variety of biospecies: (1) blank, (2) *S*-nitrosoglutathione (GSNO) (100 μM), (3) $ONOO^-$ (100 μM), (4) NO (NOC-5) (100 μM), (5) NO_2^- (100 μM), (6) tocopherols (100 μM), (7) H_2O_2 (100 μM), (8) $O_2^{\bullet-}$ (100 μM), (9) methyl linoleate hydroperoxide (100 μM), (10) Na_2S_4 (a donor of H_2S_n) (100 μM), (11) L-cysteine (L-cys) (100 μM), (12) glutathione (GSH) (100 μM), (13) NaHS (100 μM), (14) ascorbic acid (100 μM), (15) L-arginine (L-arg) (100 μM), (16) tyrosine (100 μM), (17) hydroxylamine (HA) (100 μM), (18) NaClO (30 μM). The results clearly disclose that only in the presence of HOCl, a large increase in the fluorescence signal could be observed. Under complex physiological conditions, BCy-HOCl exhibited an outstanding selectivity towards HOCl rather than other biological species.

3.5 Imaging of HOCl in living cells

Considering the excellent capability of BCy-HOCl to sense HOCl in simulated physiological environments, we then evaluated whether BCy-HOCl can sensitively detect the physiological level of HOCl in different living cells. Before the cell experiments, we first evaluated the probe biocompatibility. In the MTT assays, BCy-HOCl displayed low cytotoxicity towards A549 cells and RLE-6TN cells (Fig. S2, ESI†), which illustrated that BCy-HOCl was capable of being utilized in cell environments. BCy-HOCl was employed to evaluate the fluctuation of HOCl in living cells. All tested cells in this study were incubated with BCy-HOCl for 30 min before imaging. A faint fluorescence signal was observed in Fig. 2a, disclosing that the HOCl level in this group of cells was very low. The fluorescence intensity was much stronger when these two cell lines were stimulated with NaClO to provide exogenous HOCl (Fig. 2b). The ability of BCy-HOCl to
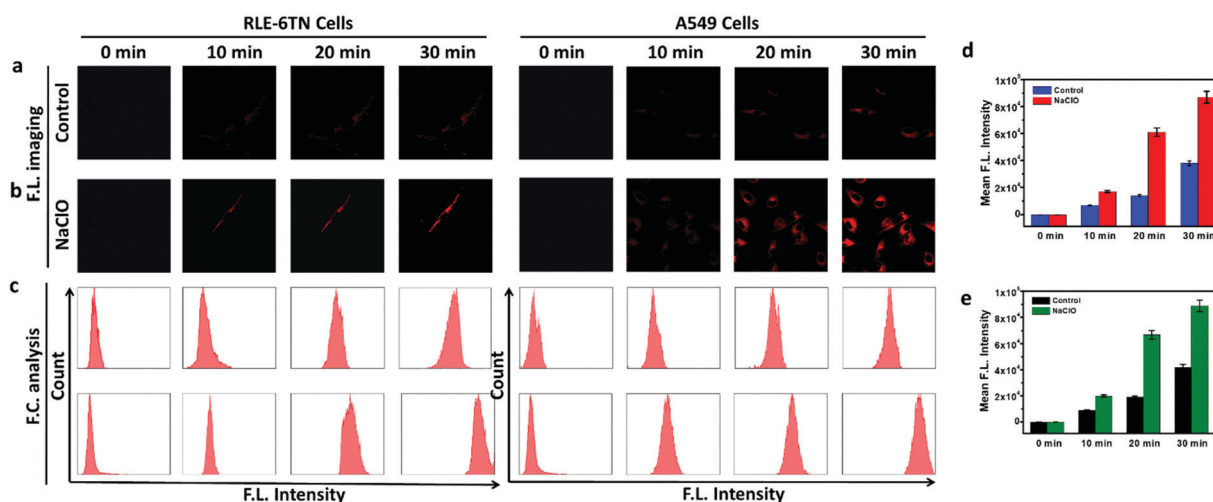

Fig. 2 Confocal microscopy images and flow cytometry assay of A549 and RLE-6TN cells for detecting the variation of HOCl in living cells. (a) Real-time HOCl detection with BCy-HOCl (5 μM) in A549 and RLE-6TN cells at different times: 0, 10, 20, and 30 min as the control. (b) Before being processed, as described in the control, A549 cells and RLE-6TN cells were treated with NaClO (50 mM) for another 15 min, respectively. (c) Flow cytometry analysis of (a and b). (d) Mean fluorescence intensity of A549 cells. (e) Mean fluorescence intensity of RLE-6TN cells. (Red channel: $\lambda_{ex} = 543$ nm, $\lambda_{em} = 600-700$ nm.) The data are displayed as mean (s.d.).

clearly monitor exogenous HOCl in living cells is confirmed by the above results. We further confirm the cell imaging results *via* flow cytometry (Fig. 2c). The mean fluorescence intensity of A549 cells and RLE-6TN cells is displayed in Fig. 2d and e. These above results confirm that BCy-HOCl is a credible tool and adequate to directly detect HOCl changes in living cells.

3.6 Imaging of HOCl in ALI cell models

Currently, there are a wide range of models available for the research of ALI. Because the most common cause of ALI in patients is still sepsis, researchers have conducted extensive research on the LPS-induced ALI model to solve the pathogenesis. It is generally considered that LPS might damage the lungs by directly affecting the cells and their capability of inducing the release of various host-derived inflammatory mediators.[40,41] Therefore, we applied the probe BCy-HOCl to monitor the variation of HOCl levels in LPS-induced ALI cell models. For the establishment of ALI cell models stimulated by LPS, A549 cells were stimulated with LPS (500 μM) for 24 h. The A549 cells were treated with BCy-HOCl for 30 min before imaging. As expected, the fluorescence of the tested cells in the LPS-induced group was much stronger than that in the control, indicating the higher HOCl levels in these cells (Fig. 3a). Using flow cytometry, we further checked the results from laser scanning confocal microscopy (Fig. 3b). Previous researches have demonstrated that the variation in the HOCl levels could be causally correlated with apoptosis.[42,43] For this reason, we accessed the apoptosis degree of A549 cells in the two different groups *via* flow cytometry, and the apoptosis degree of the LPS-induced group increased with the rate of apoptosis from almost 0.0% increased up to 42.3%, certifying that the degrees of apoptosis were positively correlated to the

levels of HOCl (Fig. 3c). The mean fluorescence intensity of cell imaging is displayed in Fig. 3g.

Hyperoxia-induced ALI, as an iatrogenic lung dysfunction, is triggered by long-term exposure to hyperoxia and commonly occurs during the treatment of refractory hypoxemia. Hyperoxia-induced ALI models have been mostly utilized as a feasible tool to induce excessive production of oxidants in lungs.[44] Prolonged exposure to hyperoxia results in the building up of ROS, thus decreasing the cell viability.[44] For the establishment of ALI cell models induced by hyperoxia, RLE-6TN cells were treated with 500 mM H_2O_2 for 8 h, 16 h, and 24 h to induce the hyperoxia exposure. Then, before imaging, the control cells and hyperoxia-induced ALI cell models were treated with BCy-HOCl for 30 min. The much stronger fluorescence of the tested cells in the hyperoxia-induced group than in the controls illustrated the higher HOCl levels in the RLE-6TN cells (Fig. 3d). The flow cytometry analysis exhibited the same trend as laser scanning confocal microscopy (Fig. 3e). The apoptosis degree of the hyperoxia-induced group has increased. The apoptosis rate of the cells in the control group was almost 0.0%, and after stimulation with H_2O_2 for 8 h, 16 h, and 24 h, the apoptosis rate of the cells increased up to 30.8%, 38.7%, and 66.4%, respectively (Fig. 3f). Fig. 3h shows the mean fluorescence intensities of cell imaging. These data certified that the HOCl level in the two types of ALI cell models obviously increased, and the intracellular HOCl level has a close correlation with ALI.

3.7 Imaging of HOCl in ALI mouse models

Since the fluctuations of HOCl in ALI cell models were demonstrated, we next disclosed the concentration changes of HOCl in the ALI mice models. The LPS-induced ALI mouse models were established *via* LPS stimulation for 0 h, 8 h, 16 h and 24 h through intranasal administration. BCy-HOCl was intratracheal administered
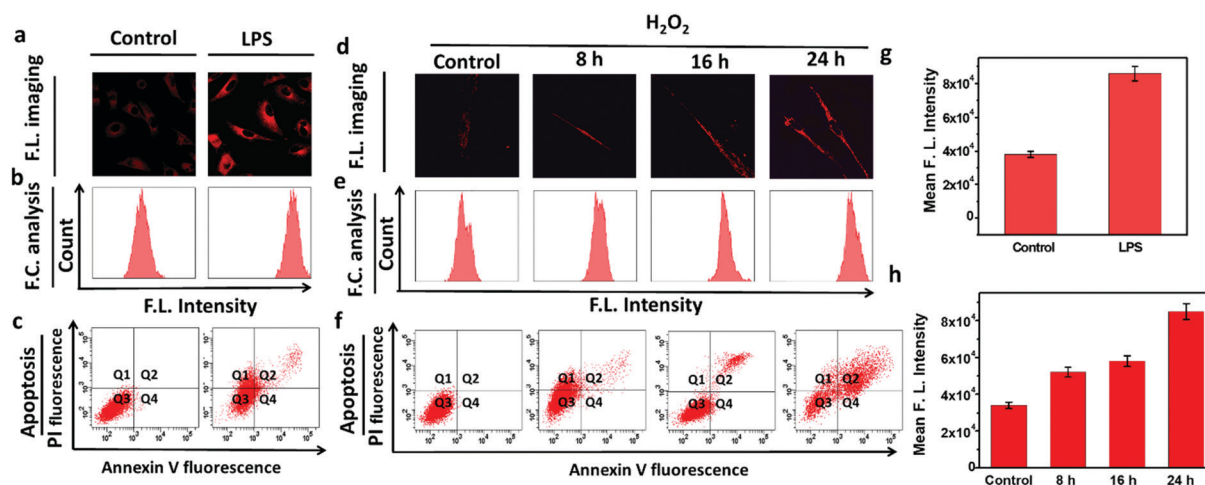

Fig. 3 The fluctuation of HOCl in ALI cell models. (a) HOCl imaging of A549 cells using BCy-HOCl (5 μM) as the control. Prior to the treatment described in the control group, in order to establish the ALI cell model, A549 cells were treated with LPS (500 μM) for 24 h. (b) Flow cytometry assay of cells in (a). (c) Apoptosis analysis of the cells in (a). (d) HOCl imaging of RLE-6TN cells using BCy-HOCl (5 μM) as the control. Prior to the treatment described in the control group, in order to induce the hyperoxia exposure, RLE-6TN cells were treated with 500 mM H_2O_2 for 24 h. (e) Flow cytometry assay of the cells in (d). (f) Apoptosis analysis of the cells in (d). (g) Mean fluorescence intensity of A549 cells. (h) Mean fluorescence intensity of RLE-6TN cells. (Red channel: λ_{ex} = 543 nm, λ_{em} = 600–700 nm.) The data are displayed as mean (s.d.).

This journal is © The Royal Society of Chemistry 2020

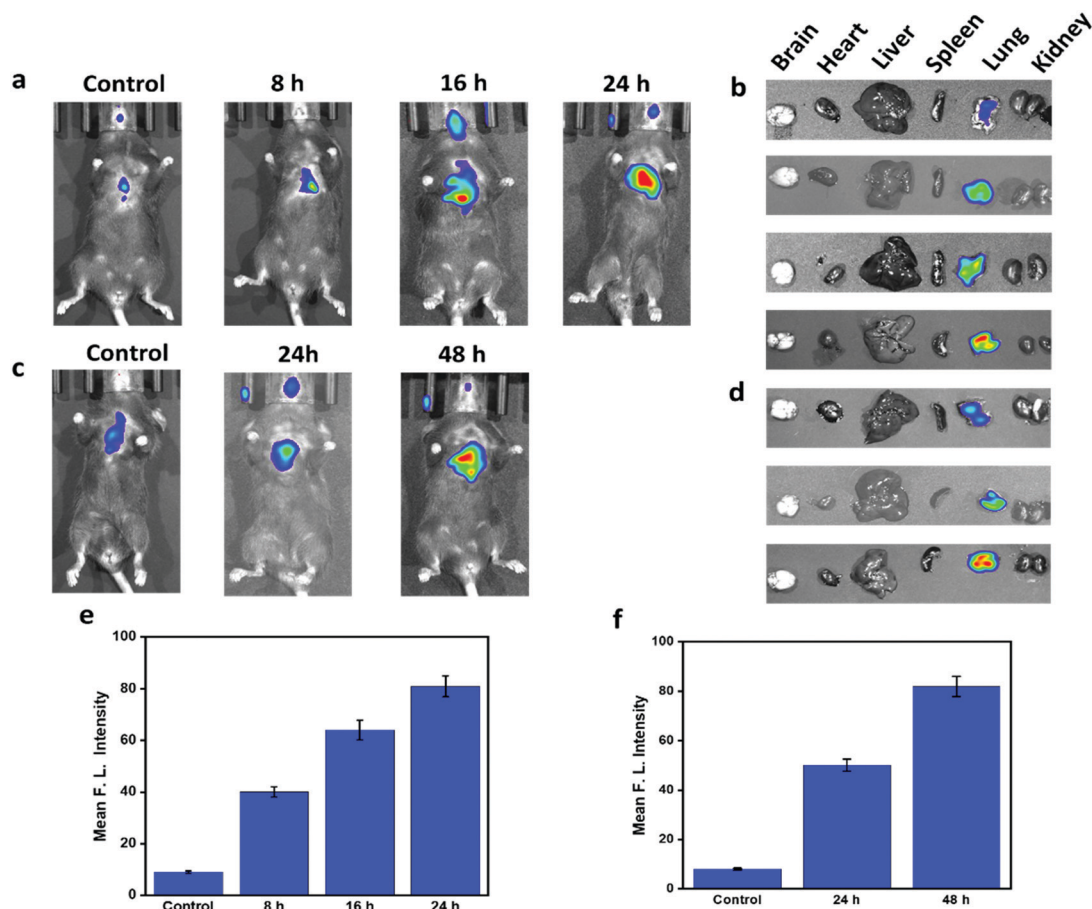*J. Mater. Chem. B*, 2020, **8**, 9899–9905 | **9903**

Fig. 4 The fluctuation of HOCl in ALI mouse models. (a) Real-time HOCl imaging in various mouse groups with multiple stimulating times by LPS: 0 h, 12 h and 24 h. (b) Imaging of isolated organs in (a). (c) Real-time HOCl imaging in various mouse groups exposed to high level of oxygen at multiple times: 0 h, 24 h and 48 h. (d) Imaging of the isolated lung in (e). (e) Mean fluorescence intensity of (a). (f) Mean fluorescence intensity of imaging (c). Fluorescence imaging channel: λ_{ex} = 543 nm, λ_{em} = 600–700 nm. Data are presented as mean ± SD (n = 5).

1 h before *in vivo* imaging. As the stimulus time increased, the fluorescence of the LPS-stimulated mice was stronger, verifying that the HOCl levels conspicuously increased with the aggravation of ALI (Fig. 4a). The fluorescence images of the isolated lung were in conformity with those assays from the *in vivo* imaging (Fig. 4b). The mean fluorescence intensities are shown in Fig. 4e. The hyperoxia-induced ALI mouse models were constructed *via* exposure to high levels of oxygen for 0 h, 24 h and 48 h. BCy-HOCl was intratracheal administered 1 h before *in vivo* imaging. With the extension of the stimulation time, the fluorescence of hyperoxia-stimulated mice increased, indicating that the HOCl level increased with the severity of ALI (Fig. 4c). The fluorescence imaging of the isolated lung clarified the change in the HOCl level (Fig. 4d). The mean fluorescence intensities are shown in Fig. 4f. The above results confirm the potential connection between the HOCl level and the degrees of ALI. HOCl may play a crucial part in the development process of ALI.

4. Conclusions

In conclusion, we have described the fluorescent probe BCy-HOCl for the evaluation of the HOCl level fluctuation in living cells and *in vivo*. BCy-HOCl was utilized to measure HOCl in two types of ALI cell models as well as for the real-time tracking of the HOCl fluctuation in two corresponding ALI animal models. With the help of BCy-HOCl, we found that the HOCl level has increased with the severity of ALI. The potential correlation between the HOCl level and the degrees of ALI are indicated. Our research provides evidence that HOCl may be a vital factor in the development process of ALI. BCy-HOCl provides a promising tool for the better detection of the physiological and pathological HOCl level in cells and *in vivo*.

Conflicts of interest

There are no conflicts to declare.

Acknowledgements

9904 | *J. Mater. Chem. B*, 2020, **8**, 9899–9905

This journal is © The Royal Society of Chemistry 2020

References

1 M. A. E. Rabelo, L. M. F. Lucinda, M. M. Reboredo, L. M. C. da Fonseca, F. F. Reis, T. F. Fazza, D. R. Brega, F. de Paoli, A. D. da Fonseca and B. V. Pinheiro, *Inflammation*, 2018, **41**, 174–182.

2 S. Luh and C. Chiang, *J. Zhejiang Univ., Sci., B*, 2007, **8**, 60–69.

3 T. C. Allen and A. Kurdowska, *Arch. Pathol. Lab. Med.*, 2014, **138**, 266–269.

4 C. A. Ruthman and E. Festic, *Ther. Adv. Respir. Dis.*, 2015, **9**, 173–187.

5 E. Hidalgo, R. Bartolome and C. Dominguez, *Chem.-Biol. Interact.*, 2002, **139**, 265–282.

6 C.-H. Sam and H.-K. Lu, *J. Dent. Sci.*, 2009, **4**, 45–54.

7 M. Casciaro, E. Di Salvo, E. Pace, E. Ventura-Spagnolo, M. Navarra and S. Gangemi, *Immun. Ageing*, 2017, **14**, 21.

8 C.-H. Sam and H.-K. Lu, *J. Dent. Sci.*, 2009, **4**, 45–54.

9 Y. W. Jun, S. Sarkar, S. Singha, Y. J. Reo, H. R. Kim, J.-J. Kim, Y.-T. Chang and K. H. Ahn, *Chem. Commun.*, 2017, **53**, 10800–10803.

10 R. Zhang, B. Song and J. Yuan, *TrAC, Trends Anal. Chem.*, 2018, **99**, 1–33.

11 Y. Yue, F. Huo, C. Yin, J. O. Escobedo and R. M. Strongin, *Analyst*, 2016, **141**, 1859–1873.

12 L. Yuan, W. Lin, Y. Xie, B. Chen and J. Song, *Chemistry*, 2012, **18**, 2700–2706.

13 B. Zhu, L. Wu, M. Zhang, Y. Wang, C. Liu, Z. Wang, Q. Duan and P. Jia, *Biosens. Bioelectron.*, 2018, **107**, 218–223.

14 H. Xiao, K. Xin, H. Dou, G. Yin, Y. Quan and R. Wang, *Chem. Commun.*, 2015, **51**, 1442–1445.

15 L. Yuan, L. Wang, B. K. Agrawalla, S. J. Park, H. Zhu, B. Sivaraman, J. Peng, Q. H. Xu and Y. T. Chang, *J. Am. Chem. Soc.*, 2015, **137**, 5930–5938.

16 Q. Xu, C. H. Heo, J. A. Kim, H. S. Lee, Y. Hu, D. Kim, K. M. Swamy, G. Kim, S. J. Nam, H. M. Kim and J. Yoon, *Anal. Chem.*, 2016, **88**, 6615–6620.

17 H. J. Lee, M. J. Cho and S. K. Chang, *Inorg. Chem.*, 2015, **54**, 8644–8649.

18 P. Chen, Z. Zheng, Y. Zhu, Y. Dong, F. Wang and G. Liang, *Anal. Chem.*, 2017, **89**, 5693–5696.

19 Q. Xu, K. A. Lee, S. Lee, K. M. Lee, W. J. Lee and J. Yoon, *J. Am. Chem. Soc.*, 2013, **135**, 9944–9949.

20 J. J. Hu, N. K. Wong, M. Y. Lu, X. Chen, S. Ye, A. Q. Zhao, P. Gao, K. R. Yi-Tsun, J. Shen and D. Yang, *Chem. Sci.*, 2016, **7**, 2094–2099.

21 S. I. Reja, V. Bhalla, A. Sharma, G. Kaur and M. Kumar, *Chem. Commun.*, 2014, **50**, 11911–11914.

22 Q. Zhang, N. Zhang, Y. T. Long, X. Qian and Y. Yang, *Bioconjugate Chem.*, 2016, **27**, 341–353.

23 M. Emrullahoglu, M. Ucuncu and E. Karakus, *Chem. Commun.*, 2013, **49**, 7836–7838.

24 H. Zhu, J. Fan, J. Wang, H. Mu and X. Peng, *J. Am. Chem. Soc.*, 2014, **136**, 12820–12823.

25 G. Cheng, J. Fan, W. Sun, J. Cao, C. Hu and X. Peng, *Chem. Commun.*, 2014, **50**, 1018–1020.

26 J. J. Hu, N. K. Wong, Q. Gu, X. Bai, S. Ye and D. Yang, *Org. Lett.*, 2014, **16**, 3544–3547.

27 G. Cheng, J. Fan, W. Sun, K. Sui, X. Jin, J. Wang and X. Peng, *Analyst*, 2013, **138**, 6091–6096.

28 J. T. Hou, K. Li, J. Yang, K. K. Yu, Y. X. Liao, Y. Z. Ran, Y. H. Liu, X. D. Zhou and X. Q. Yu, *Chem. Commun.*, 2015, **51**, 6781–6784.

29 H. Feng, Z. Zhang, Q. Meng, H. Jia, Y. Wang and R. Zhang, *Adv. Sci.*, 2018, **5**, 1800397.

30 L. Cao, R. Zhang, W. Zhang, Z. Du, C. Liu, Z. Ye, B. Song and J. Yuan, *Biomaterials*, 2015, **68**, 21–31.

31 F. Zhang, X. Liang, W. Zhang, Y. L. Wang, H. Wang, Y. H. Mohammed, B. Song, R. Zhang and J. Yuan, *Biosens. Bioelectron.*, 2017, **87**, 1005–1011.

32 Y. L. Pak, S. J. Park, G. Song, Y. Yim, H. Kang, H. M. Kim, J. Bouffard and J. Yoon, *Anal. Chem.*, 2018, **90**, 12937–12943.

33 Q. Duan, P. Jia, Z. Zhuang, C. Liu, X. Zhang, Z. Wang, W. Sheng, Z. Li, H. Zhu, B. Zhu and X. Zhang, *Anal. Chem.*, 2019, **91**, 2163–2168.

34 B. Zhu, L. Wu, M. Zhang, Y. Wang, Z. Zhao, Z. Wang, Q. Duan, P. Jia and C. Liu, *Sens. Actuators, B*, 2018, **263**, 103–108.

35 B. Zhu, L. Wu, H. Zhu, Z. Wang, Q. Duan, Z. Fang, P. Jia, Z. Li and C. Liu, *Sens. Actuators, B*, 2018, **269**, 1–7.

36 C. Liu, P. Jia, L. Wu, Z. Li, H. Zhu, Z. Wang, S. Deng, W. Shu, X. Zhang, Y. Yu and B. Zhu, *Sens. Actuators, B*, 2018, **297**, 126731.

37 C. Liu, Z. Li, C. Yu, Y. Chen, D. Liu, Z. Zhuang, P. Jia, H. Zhu, X. Zhang, Y. Yu, B. Zhu and W. Sheng, *ACS Sens.*, 2019, **4**, 2156–2163.

38 H. Zhang, R. Liu, Y. Tan, W. H. Xie, H. Lei, H. Y. Cheung and H. Sun, *ACS Appl. Mater. Interfaces*, 2015, **7**, 5438–5443.

39 H. Li, L. Guan, X. Zhang, H. Yu, D. Huang, M. Sun and S. Wang, *Talanta*, 2016, **161**, 592–598.

40 D. D. Bannerman and S. E. Goldblum, *Am. J. Physiol.: Lung Cell. Mol. Physiol.*, 2003, **284**, L899–L914.

41 M. Bhatia and S. Moochhala, *J. Pathol.*, 2004, **202**, 145–156.

42 M. C. M. Vissers, J. M. Pullar and M. B. Hampton, *Biochem. J.*, 1999, **344**, 443–449.

43 J. M. Pullar, M. C. M. Vissers and C. C. Winterbourn, *IUBMB Life*, 2000, **50**, 259–266.

44 C. G. Cochrane, R. Spragg and S. D. Revak, *J. Clin. Invest.*, 1983, **71**, 754–761.